Infrared Frequency-Modulation Probing of Product Formation in Alkyl + O_2 Reactions: I. The Reaction of C_2H_5 with O_2 between 295 and 698 K

Eileen P. Clifford,[†,‡] John T. Farrell,[†,§] John D. DeSain,[†] and Craig A. Taatjes*

Combustion Research Facility, Mail Stop 9055, Sandia National Laboratories, Livermore, California 94551-0969

Received: July 12, 2000; In Final Form: October 3, 2000

The production of HO_2 in the reaction of ethyl radicals with molecular oxygen has been investigated using laser photolysis/cw infrared frequency modulation spectroscopy. The ethyl radicals are formed by reaction of photolytically produced Cl atoms with ethane, initiated via pulsed laser photolysis of Cl_2, and the progress of the reaction is monitored by frequency-modulation spectroscopy of the HO_2 product. The yield of HO_2 in the reaction is measured by comparison with the $Cl_2/CH_3OH/O_2$ system, which quantitatively converts Cl atoms to HO_2. At low temperatures stabilization to $C_2H_5O_2$ dominates, but at elevated temperatures (> 575 K) dissociation of the ethylperoxy radical begins to contribute. Biexponential time behavior of the HO_2 production allows separation of prompt, "direct" HO_2 formation from HO_2 produced after thermal redissociation of an initial ethylperoxy adduct. The prompt HO_2 yield exhibits a smooth increase with increasing temperature, but the total HO_2 yield, which includes contributions from the redissociation of ethylperoxy radicals, rises sharply from ∼10% to 100% between 575 and 675 K. Because of the separation of time scales in the HO_2 production, this rapid rise can unambiguously be assigned to ethylperoxy dissociation. No OH was observed in the reaction, and an upper limit of 6% can be placed on direct OH formation from the $C_2H_5 + O_2$ reaction at 700 K. The time behavior of the HO_2 production is at variance with the predictions of Wagner et al.'s RRKM-based parameterization of this reaction (*J. Phys. Chem.* **1990**, *94*, 1853). However, a simple ad hoc correction to that model, which takes into account a recent reinterpretation of the equilibrium constant for $C_2H_5 + O_2 \leftrightarrow C_2H_5O_2$, predicts yields and time constants consistent with the present measurements. The reaction mechanism is further discussed in terms of recent quantum chemical and master equation studies of this system, which show that the present results are well described by a coupled mechanism with $HO_2 + C_2H_4$ formed by direct elimination from the $C_2H_5O_2$ adduct.

Reactions of alkyl radicals with oxygen molecules are critical in understanding many combustion systems and play an especially important role in autoignition phenomena. At low temperatures, stabilization to the alkylperoxy radical dominates the reaction. At higher temperatures, thermal dissociation of the alkylperoxy radical becomes more rapid and only bimolecular product channels remain. This change in mechanism is responsible for the negative temperature coefficient region in hydrocarbon oxidation. Depending on the size of the alkyl radical, reaction with O_2 can lead to either HO_2 radicals and the conjugate alkene or to the more reactive OH radical and an epoxide. The precise mechanism of these reactions has been a source of puzzlement, with apparently contradictory conclusions arising from investigations of the forward and the reverse (HO_2 + alkene) reactions. The reaction of ethyl radicals with O_2 has been the most extensively studied of all the R + O_2 reactions, with a wealth of theoretical and experimental investigations. Ethyl + O_2 has been regarded as prototypical for the set of R + O_2 reactions, a position gained mainly from its relative theoretical tractability; it is the smallest R + O_2 system for which HO_2 + alkene and OH + epoxide formation are possible.

Previous experiments on the ethyl + O_2 reaction have determined that at low temperatures the ethyl radical forms an adduct with the oxygen which may be collisionally stabilized. At higher temperatures and lower pressures the bimolecular product channels, principally to ethylene + HO_2, increase in importance.

$$C_2H_5 + O_2 \xleftrightarrow{[M]} C_2H_5O_2 \quad (1a)$$

$$\rightarrow C_2H_4 + HO_2 \quad (1b)$$

$$\rightarrow c - C_2H_4O(\text{oxirane}) + OH \quad (1c)$$

Much of the investigation of ethyl + O_2 has concentrated on unraveling the mechanism of the reaction.[1−3] Proposed mechanisms have generally fallen into two categories, a parallel mechanism and a coupled mechanism. The parallel mechanism typically postulates an activated direct abstraction mechanism for the production of C_2H_4, which would occur as a parallel path to stabilization. The coupled mechanism proposes that formation of a vibrationally excited ethylperoxy adduct is the initial step toward formation of all of the observed products. Reactions 1b and 1c therefore occur by rearrangement and

[†] Sandia National Laboratories Postdoctoral Associate.

[‡] Present address: Therma-Wave Inc., 1250 Reliance Way, Fremont, CA 94539.

[§] Present address: Exxon Mobil Research and Engineering Company, 1545 Route 22 East, LH386, Annandale, NJ 08801.

* To whom correspondence should be addressed.

10.1021/jp0024874 CCC: $19.00
Published on Web 11/17/2000

dissociation of the ethylperoxy adduct, and all product channels are coupled through reaction 1a. These two types of reaction mechanism imply different effects of temperature and pressure on the rate coefficient and branching fractions for reaction 1.

The available experimental evidence appears to favor some form of the coupled mechanism for reaction 1 at temperatures below 1000 K. The reaction produces $C_2H_4 + HO_2$ even at room temperature, with a yield that decreases with increasing pressure. Early measurements by Plumb and Ryan suggested a pressure-independent component to C_2H_4 formation,[4] as would be observed in a parallel mechanism. However, more recent measurements by Kaiser, Wallington, and co-workers have shown a $(pressure)^{-0.8}$ dependence of the C_2H_4 yield over nearly 4 orders of magnitude and have demonstrated that the pressure-independent contribution to C_2H_4 is negligible.[5−7] Slagle, Feng, and Gutman showed that the consumption of C_2H_5 in reaction 1 exhibits a negative temperature dependence from 298 to 1000 K,[8] even at temperatures > 700 K where the yield of C_2H_4 is essentially unity, a result which has been corroborated by McAdam and Walker.[9] McAdam and Walker found that formation of C_2H_4 dominates the $C_2H_5 + O_2$ reaction between 673 and 813 K, with only a small branching to $OH + c\text{-}C_2H_4O$ products. The observed negative temperature dependence precludes an activated direct abstraction mechanism for reaction 1b. Significant abstraction contributions are to be expected only at still higher temperatures.

The details of the coupled reaction mechanism have been a source of greater controversy. Reaction of the $C_2H_5O_2$ radical is thought to pass through a cyclic five membered transition state before forming products. It was initially proposed that isomerization to an ethyl hydroperoxy radical is the initial step in the formation of HO_2 and C_2H_4. To account for the negative temperature dependence, the transition state for this isomerization must lie below the energy of $C_2H_5 + O_2$. A QRRK calculation by Bozzelli and Dean predicted that isomerization to the ethylhydroperoxy radical (C_2H_4OOH) would be followed rapidly by dissociation to $C_2H_4 + HO_2$.[10] Wagner et al. developed a model in 1990 which parameterizes the experimental evidence for the forward reaction using a similar mechanism, with a transition state for isomerization lying 2.4 kcal mol^{-1} below ethyl + O_2.[11] The exact nature of the pathway from C_2H_5OO to $HO_2 + C_2H_4$ is not constrained by the experimental measurements used in Wagner et al.'s RRKM fits, except for requiring rapid irreversible dissociation of any intermediate species to products.

However, investigations by Walker and co-workers of the reverse reaction, $HO_2 + C_2H_4$, suggested a barrier of 17 kcal mol^{-1} for the addition to form C_2H_4OOH, and a still higher barrier for the isomerization to C_2H_5OO. Further, the $HO_2 + C_2H_4$ reaction was observed to form principally $c\text{-}C_2H_4O + OH$ instead of $C_2H_5 + O_2$.[12,13] These measurements appeared to rule out C_2H_4OOH as an intermediate species in the formation of C_2H_4 and HO_2 in reaction 1. An alternative mechanism for reaction 1b has been proposed, with a cyclic transition state leading to direct HO_2 elimination from $C_2H_5O_2$. Calculations at various levels of theory have confirmed this proposal,[14−16] with recent density functional calculations producing a cyclic transition state for HO_2 elimination 1.9 kcal mol^{-1} below the reactants. Miller, Klippenstein, and Robertson have performed time-dependent master equation simulations of reaction 1 using ab initio theory to characterize the important stationary points on the potential energy surface.[17] They calculate the HO_2 elimination transition state as −3.0 kcal mol^{-1} relative to the reactants, in good agreement with the −4.3 kcal mol^{-1} they infer from comparison of the master equation results to experimental data. While this transition state may account for the behavior of the $C_2H_5 + O_2$ reaction, an explanation which also predicts the preferential production of C_2H_4OOH from the $C_2H_4 + HO_2$ reaction, with a sizable activation barrier, remains elusive. Recent ab initio and density functional calculations yield a smaller activation energy (∼13.5 kcal mol^{-1}) for HO_2 addition to ethylene than that deduced by Walker's group.[18] The apparent disharmony between measurements of the forward and reverse reaction may be alleviated by recent proposals involving the participation of excited electronic surfaces.[1−3]

Several experimental investigations of the ethyl + O_2 reaction have concentrated on describing the fate of the ethylperoxy radical in the coupled mechanism. Slagle et al. have studied the kinetics and probable mechanism of the $C_2H_5 + O_2$ reaction in a series[8,19,20] of papers, observing production of ethylene and HO_2 as well as the $C_2H_5O_2$ adduct, and measuring thermochemical bond strengths and kinetic rate coefficients. A detailed analysis of this experimental data, along with a fit to an RRKM model, forms the basis for the parameterization of Wagner et al.[11] Recently, Kaiser has studied the ethylene branching fraction as a function of temperature and pressure.[21] In these experiments, the total yield of C_2H_4 is determined using end-product analysis from photolysis of $Cl_2/C_2H_6/O_2$ mixtures in a smog chamber apparatus. The yield of C_2H_4 as a function of temperature displays a slow increase with temperature from ambient up to ∼400 K, followed by a more rapid increase around 500 K. The rapid increase is attributed to the onset of thermal decomposition of the ethylperoxy radical, and Kaiser is able to fit his data using a 12-reaction model, employing the Wagner et al. parameterization for the ethyl + O_2 reaction.

In the present investigation, infrared frequency-modulation spectroscopy is used to monitor the time behavior of HO_2 production from reaction 1 as a function of pressure and temperature. Using the time resolution in these experiments, it is possible to discern the kinetic signature of the equilibration in reaction 1a. Redissociation of the $C_2H_5O_2$ regenerates the reactants after some delay, resulting in a biexponential profile of HO_2 production. The difference in time scales permits a separation between "prompt" HO_2 and HO_2 which is produced after ethylperoxy redissociation. The time behavior of HO_2 production from ethylperoxy dissociation has also been measured as a function of temperature and pressure. These observations are complementary to the lower pressure measurements of reactant disappearance by Slagle, Gutman, and co-workers[8,11,19,20] and the final product measurements of Kaiser et al.,[5−7,21] and provide an additional level of detailed experimental characterization of this critical combustion reaction. The present total yield measurements can be qualitatively modeled using the parameterization of Wagner et al.,[11] with modifications to account for recent improvements in the equilibrium constants for reaction 1a.[19] The detailed time behavior is in excellent agreement with recent master equation calculations.[17]

Experiment

The reaction of C_2H_5 with O_2 is investigated using a modification of the laser photolysis/continuous wave (CW) infrared long-path absorption (LP/CWIRLPA) method, similar to that employed in previous experiments.[22−26] The reaction is initiated by pulsed photolysis of Cl_2 at 355 nm. The Cl atoms react rapidly with a large excess of ethane (99.995% purity) to

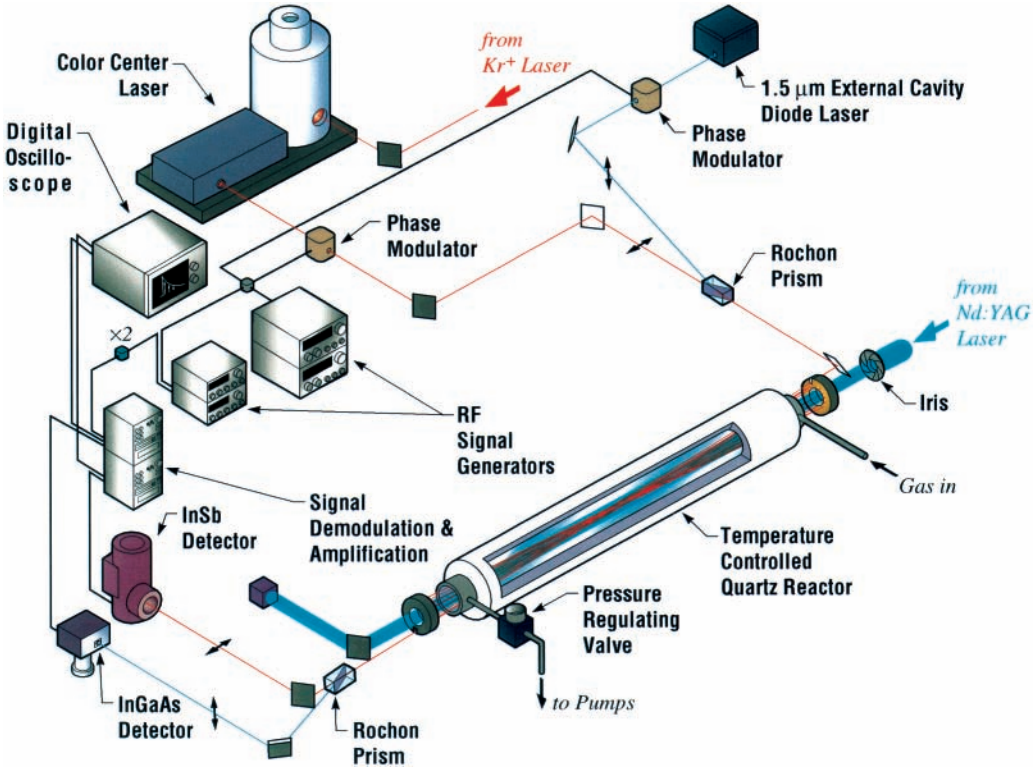

Figure 1. Diagram of the experimental apparatus.

produce the corresponding C_2H_5 radical in a nearly thermoneutral reaction. The thermal C_2H_5 subsequently reacts with O_2.

$$Cl_2 \xrightarrow{h\nu(355\ nm)} 2Cl\bullet \quad (2)$$

$$Cl + C_2H_6 \rightarrow C_2H_5 + HCl \quad (3)$$

$$C_2H_5 + O_2 \rightarrow \text{products} \quad (1)$$

The progress of reaction 1 is monitored by infrared absorption of the overtone of the O−H stretch in HO_2 near 6686 cm^{-1} using a tunable diode laser.[27−29] Possible OH production is monitored by absorption on the P(2.5)1$^-$ line of the vibrational fundamental[30] at 3484.6 cm^{-1} using an F-center laser. Two-tone frequency modulation of the infrared lasers is sometimes employed[26,31] to increase the signal-to-noise ratio. The sensitivity decreases at higher temperatures due to increases in the vibrational and rotational partition functions. The infrared probe beams are passed multiple times through the reactor using a Herriott-type multipass cell.[32,33] The optical arrangement is depicted in Figure 1. Both infrared beams are placed on the same path through the reactor using polarizing prisms to combine and separate the beams. The Nd:YAG photolysis laser (2−3 mJ cm^{-2}) travels along the axis of the cell, and the pump−probe overlap is confined to the center of the cell, where the temperature can be precisely controlled.

The relative yield of HO_2 in the reaction of C_2H_5 with O_2 is determined by comparison with the reference reaction of CH_2OH with oxygen, which produces one HO_2 for each CH_2OH.[34] Signals are acquired using the same amount of Cl_2 and the same photolysis conditions, but replacing the ethane flow by a similar flow of methanol. The initial Cl concentration is the same in both cases, and the amount of HO_2 produced from the ethane reaction can be scaled to the 100% conversion of Cl to HO_2 in reactions 4 and 5 by comparing signal strengths.

$$Cl_2 \xrightarrow{h\nu(355\ nm)} 2Cl\bullet \quad (2)$$

$$Cl + CH_3OH \xrightarrow{100\%} CH_2OH + HCl \quad (4)$$

$$CH_2OH + O_2 \xrightarrow{100\%} HO_2 + CH_2O \quad (5)$$

The yield of OH can be determined using the same reference reaction, by completely reacting HO_2 with NO to form OH radicals.[35]

$$HO_2 + NO \xrightarrow{100\%} OH + NO_2 \quad (6)$$

Comparison of the signal amplitudes of HO_2 or OH from reaction with ethane to that of the reference reaction with methanol gives a phenomenological yield of the products. To relate the observed quantities to characteristics of the reaction, corrections must be made for removal reactions of OH and HO_2, as well as for certain side reactions, as discussed below.

The individual gas flows are controlled by calibrated mass flow controllers, and the chosen total pressure is maintained by a butterfly valve at the exit of the cell which operates under feedback from a capacitance manometer. The reactor is heated by three resistive elements, each under microprocessor control from a separate K-type thermocouple. The pressure using the present yield measurement method is limited to about 100 Torr, above which the neat methanol vapor does not produce a stable flow. Typical concentrations are $[O_2] = 10^{17}$ molecules cm^{-3}; $[Cl_2] = 10^{15}$ molecules cm^{-3}; and $[C_2H_6]$ or $[CH_3OH] = 5 \times 10^{15}$ molecules cm^{-3}, with the remainder He (99.9999%). In the reference system for OH detection NO concentrations of $\sim 4 \times 10^{14}$ cm^{-3} are typically used. The reaction of ethyl with Cl_2 can affect the production of HO_2 by sequestering radical density in the Cl_2/C_2H_6 chain reaction, causing incorrect yield

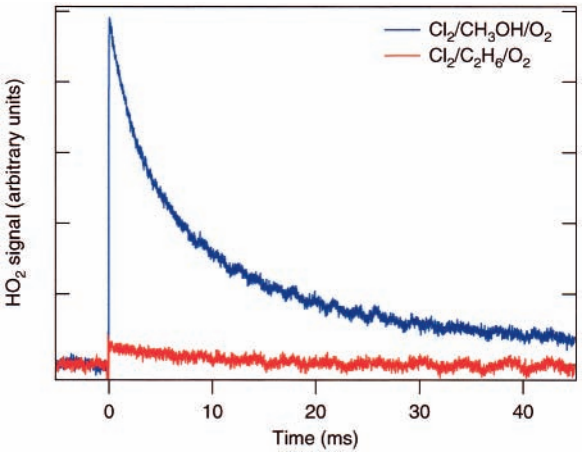

Figure 2. Time-resolved HO_2 signals taken at 423 K. The larger amplitude trace in blue is the HO_2 signal from the reference reaction; the smaller amplitude trace in red is the HO_2 signal from the $Cl_2/C_2H_6/O_2$ system.

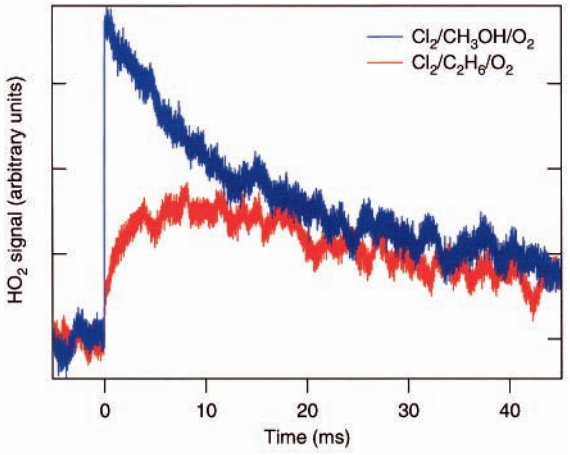

Figure 3. Time-resolved infrared FM signals for HO_2 taken at 648 K. The larger amplitude trace in blue is the HO_2 signal from the reference reaction; the smaller amplitude trace in red is the HO_2 signal from the $Cl_2/C_2H_6/O_2$ system.

measurements. Keeping the concentration of O_2 approximately 30 times higher than that of Cl_2 gives a yield that does not vary as the O_2/Cl_2 ratio increases further. The O_2 number density is maintained at 30−100 times the Cl_2 number density in order to minimize contributions from the $C_2H_5 + Cl_2$ side reaction. At the concentrations used, the reaction of Cl with ethane or methanol is complete in a few microseconds.

Results and Data Analysis

Yields of HO_2. The time-resolved production of HO_2 in reaction 1b has been measured as a function of pressure and temperature. Figure 2 shows a typical time-resolved FM signal of HO_2 at low temperature. The HO_2 FM signal from the reference reactions 4 and 5 is the larger-amplitude trace; the smaller-amplitude signal represents the smaller HO_2 yield for reaction 1 at this temperature and pressure. The reference reaction of CH_2OH with O_2 proceeds rapidly and produces HO_2 directly, and the decay of the HO_2 concentration is dominated by self-reaction. At temperatures below 550 K, the time profile of the HO_2 production from reaction 1 is similar to that from the reference reaction, that is, essentially instantaneous at the high O_2 concentrations used. Under these conditions, where the production of HO_2 is much faster than its removal, the HO_2 yield is straightforwardly calculable as the ratio of the prompt signal amplitudes.

Figure 3 shows an analogous pair of traces taken at higher temperature (648 K). The time behavior of the HO_2 produced in the reference reaction is similar to that observed at lower temperatures. Once again the HO_2 is produced rapidly and the decay is second order, principally by self-reaction. However, the production of HO_2 from reaction 1 now displays two clearly separated components. The prompt HO_2 observed at lower temperatures remains, but a slower "delayed" production of HO_2 begins to appear. The separation of time scales between production and removal of HO_2, which simplifies the prompt yield analysis, is no longer valid. Determining the fraction of HO_2 that appears via this delayed mechanism requires correction for the ongoing removal of HO_2 by self-reaction and reaction with other radical species.

This correction is accomplished using a modification of Yamasaki's integrated profiles method, originally developed to extract rate coefficients for state-to-state vibrational energy transfer.[36−38] The decay of the reference signal is dominated by the HO_2 self-reaction

$$HO_2 + HO_2 \rightarrow \text{products} \tag{7}$$

and the time profile of the HO_2 signal from the reference reaction is therefore given by

$$I_{ref}(t) = \alpha[HO_2]_t = \frac{\alpha[HO_2]_0}{1 + 2k_7[HO_2]_0 t} \tag{8}$$

with α a constant relating HO_2 concentration to FM signal amplitude. A plot of the inverse of the reference HO_2 signal vs time therefore gives a line with slope $2k_7/\alpha$. The differential equation governing the HO_2 concentration in the ethyl + O_2 reaction can be written

$$\frac{d}{dt}[HO_2] = R_{production} - 2k_7[HO_2]^2 - R_{removal}[HO_2] \tag{10}$$

where $R_{production}$ and $R_{removal}$ are the effective time-dependent rate of HO_2 production and the effective time-dependent rate coefficient for removal of HO_2 by processes besides self-reaction. Under the conditions of the present experiments, $R_{removal}$ reflects principally reactions of HO_2 with $C_2H_5O_2$ radicals,

$$HO_2 + C_2H_5O_2 \rightarrow \text{products} \tag{11}$$

so that $R_{removal} \approx k_{11}[C_2H_5O_2]_t$. Determining the time-resolved production of HO_2 from reaction 1, denoted $R_{production}$, is the aim of the measurement. Equation 10 has the formal solution

$$[HO_2]_t = \int_0^t R_{production}(x)dx - 2k_7\int_0^t [HO_2]_x^2 dx - \int_0^t R_{removal}(x)[HO_2]_x dx \tag{12}$$

So the time-dependent FM signal from HO_2 produced in reaction 1 can be described by

$$I(t) = \alpha\int_0^t R_{production}(x)dx - 2\alpha k_7\int_0^t [HO_2]_x^2 dx - \alpha\int_0^t R_{removal}(x)[HO_2]_x dx \tag{13}$$

The integrated profiles method uses this formal solution along with the measured time-resolved relative concentrations to

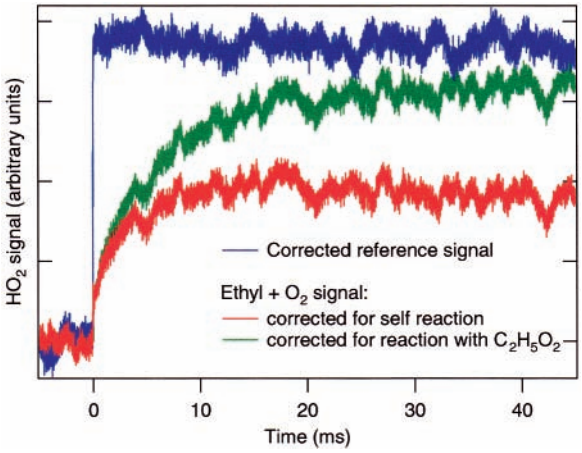

Figure 4. Correction of HO_2 FM signals from Figure 3 using the integrated profiles method. The largest-amplitude trace in blue is the HO_2 signal from the reference reaction after correction for the HO_2 self-reaction; since the decay of HO_2 in this system is dominated by the self-reaction, the signal after this correction is nearly a step function at the time of the photolysis pulse. The red trace is the HO_2 signal from the $C_2H_5 + O_2$ reaction after correction for the self-reaction; the green trace represents the signal after accounting for both the self-reaction and the reaction with $C_2H_5O_2$ radicals as described in the text. This signal represents the time-resolved production of HO_2 corresponding to the observed time-resolved FM signal.

correct for known rate processes.[37] In the present case, $2k_7/\alpha$ is known from the reference reaction, and the time profile of the HO_2 FM signal from reaction 1 has been measured: $I(t) = \alpha[HO_2]_t$. The self-reaction term in the expression for the FM signal amplitude, the second term on the right in eq 13, is thus simply related to the time integral of the observed signal

$$2\alpha k_7 \int_0^t [HO_2]_x^2 dx = \frac{2k_7}{\alpha} \int_0^t I(x)^2 dx \qquad (14)$$

The contribution of self-reaction is readily removed from the observed signals by this method. Figure 4 shows the application of this method to the raw data traces displayed in Figure 3. The reference signal now displays a rapid rise which abruptly levels off, since the production of HO_2 is extremely rapid and self-reaction is the dominant removal mechanism. The signal from reaction 1 maintains its biexponential behavior, but now also reaches a plateau at long times. If self-reaction would dominate HO_2 removal in the ethyl + O_2 system, the yield would simply be the ratio of the amplitudes of these two signals at long-time. The raw yields of HO_2 Φ_{raw}, calculated after correction for self-reaction in this manner, are listed in Table 1 along with the prompt HO_2 yields Φ_{prompt}, i.e., the ratio of the amplitudes for the fast initial rise in the ethane and methanol systems.

While the data necessary for removing the contributions of HO_2 self-reaction are inherent in the measurements themselves, relating the phenomenological yields to the time-dependent HO_2 production rate requires additional modeling. For example, under conditions where ethylperoxy and HO_2 are both present (i.e., at intermediate yields of HO_2), an additional correction is needed for the $C_2H_5O_2 + HO_2$ reaction. Correction for removal of HO_2 by the reaction with $C_2H_5O_2$ requires the relative value for the rate coefficients k_{11}/k_7, as well as information on the concentration of $C_2H_5O_2$. While literature values are available for rate coefficients of the relevant reactions, there is no direct measure of the time behavior of the ethylperoxy radical concentration. The inclusion of an additional loss channel will serve to slightly increase the yield extracted from the data. An upper limit can be constructed by assuming that all ethyl radicals react promptly to produce either HO_2 or $C_2H_5O_2$. This assumption is good if the steady-state for reaction 1a favors the products, which is the case under the high-$[O_2]$ conditions of the present experiments. Then, immediately after the fast establishment of the steady-state concentration $[C_2H_5O_2] \approx [C_2H_5]_0 - [HO_2]$. Using reactions 1, 7, 11, and the self-reaction of the ethylperoxy radical,

$$C_2H_5O_2 + C_2H_5O_2 \rightarrow \text{products} \qquad (15)$$

a formal solution to the kinetic equations can be constructed which allows recursive extraction of a corrected HO_2 profile:

$$\frac{d[C_2H_5O_2]}{dt} = -R_{production}(t) - k_{15}[C_2H_5O_2]^2 - k_{11}[HO_2][C_2H_5O_2] \qquad (16)$$

$$[C_2H_5O_2]_t = [C_2H_5]_0 - \int_0^t R_{production}(x)dx - k_{15}\int_0^t [C_2H_5O_2]^2 dx - k_{11}\int_0^t [C_2H_5O_2][HO_2]dx \qquad (17)$$

TABLE 1: Yields and Time Constants for HO_2 Production from $C_2H_5 + O_2$[a]

temp (K)	total density	Φ_{prompt}	Φ_{raw}	Φ_{total}	τ
294	3.3×10^{17} cm^{-3}	0.08	0.08	0.08	
294	8.2×10^{17} cm^{-3}	0.06	0.06	0.06	
294	1.6×10^{18} cm^{-3}	0.032	0.032	0.03	
294	2.5×10^{18} cm^{-3}	0.025	0.025	0.025	
423	1.1×10^{18} cm^{-3}	0.06	0.06	0.06	
523	4.6×10^{17} cm^{-3}	0.10	0.10	0.10	
523	9.2×10^{17} cm^{-3}	0.08	0.08	0.08	
523	1.1×10^{18} cm^{-3}	0.07	0.07	0.07	
523	1.4×10^{18} cm^{-3}	0.05	0.05	0.05	
573	7.7×10^{17} cm^{-3}	0.12	0.12	0.35	
573	1.1×10^{18} cm^{-3}	0.06	0.06	0.23	32 s^{-1}
598	7.8×10^{17} cm^{-3}	0.15	0.15	0.50	88 s^{-1}
598	9.0×10^{17} cm^{-3}	0.08	0.08	0.36	42 s^{-1}
598	1.1×10^{18} cm^{-3}	0.08	0.15	0.43	49 s^{-1}
608	9.0×10^{17} cm^{-3}	0.10	0.12	0.56	48 s^{-1}
623	3.8×10^{17} cm^{-3}	0.18	0.15	0.64	64 s^{-1}
623	5.3×10^{17} cm^{-3}	0.13	0.13	0.62	47 s^{-1}
623	6.8×10^{17} cm^{-3}	0.09	0.17	0.70	35 s^{-1}
623	7.8×10^{17} cm^{-3}	0.16	0.25	0.69	91 s^{-1}
623	8.3×10^{17} cm^{-3}	0.10	0.12	0.72	22 s^{-1}
623	9.0×10^{17} cm^{-3}	0.15	0.22	0.76	65 s^{-1}
623	1.1×10^{18} cm^{-3}	0.12	0.37	0.73	70 s^{-1}
623	1.6×10^{18} cm^{-3}	0.09	0.61	0.90	67 s^{-1}
643	1.5×10^{17} cm^{-3}	0.44	0.90	0.93	74 s^{-1}
643	3.8×10^{17} cm^{-3}	0.26	0.22	0.76	88 s^{-1}
643	7.5×10^{17} cm^{-3}	0.16	0.40	0.85	105 s^{-1}
643	8.3×10^{17} cm^{-3}	0.13	0.28	0.66	36 s^{-1}
643	9.8×10^{17} cm^{-3}	0.09	0.45	0.84	144 s^{-1}
643	1.1×10^{18} cm^{-3}	0.07	0.32	0.87	127 s^{-1}
648	3.7×10^{17} cm^{-3}	0.29	0.30	0.82	89 s^{-1}
648	7.5×10^{17} cm^{-3}	0.18	0.50	0.84	156 s^{-1}
648	7.8×10^{17} cm^{-3}	0.21	0.23	0.75	149 s^{-1}
648	9.0×10^{17} cm^{-3}	0.16	0.38	0.85	121 s^{-1}
648	1.1×10^{18} cm^{-3}	0.15	0.88	1.00	214 s^{-1}
658	8.5×10^{17} cm^{-3}	0.21	0.42	0.80	139 s^{-1}
663	3.6×10^{17} cm^{-3}	0.31	0.23	0.69	183 s^{-1}
663	6.6×10^{17} cm^{-3}	0.26	0.40	0.78	101 s^{-1}
663	8.0×10^{17} cm^{-3}	0.16	0.56	0.88	131 s^{-1}
663	1.1×10^{18} cm^{-3}	0.15	0.59	0.81	180 s^{-1}
673	5.7×10^{17} cm^{-3}	0.32	0.76	0.93	367 s^{-1}
673	7.8×10^{17} cm^{-3}	0.24	0.35	0.77	247 s^{-1}
673	9.3×10^{17} cm^{-3}	0.22	0.96	1.02	403 s^{-1}
673	1.2×10^{18} cm^{-3}	0.17	0.98	0.99	338 s^{-1}
698	7.8×10^{17} cm^{-3}	0.29	0.47	0.81	421 s^{-1}

[a] Numbers are averages for several measurements at each listed set of conditions. Estimated relative uncertainties are ± 10% for yields, ± 20% for time constants.

The equation for the observed HO_2 FM signal is modified to reflect that $k_{removal}$ is dominated by reaction with ethylperoxy radicals:

$$I(t) = \alpha\int_0^t R_{production}(x)/dx - 2\alpha k_7\int_0^t [HO_2]_x^2 dx - \alpha k_{11}\int_0^t [C_2H_5O_2]_x[HO_2]_x dx \quad (18)$$

Recognizing that the peak HO_2 signal from the methanol reference system is $I_{ref}(0) = \alpha[C_2H_5]_0$ and the quantity $2k_7/\alpha$ is known from fitting the second-order decay of the reference signal, it is straightforward to recast the kinetic equations as equations using the observed signals (i.e., effectively using signal amplitude as a concentration unit)

$$\alpha[C_2H_5O_2]_t = I_{ref}(0) - \alpha\int_0^t R_{production}(x)dx - \frac{2k_{15}}{\alpha}\int_0^t \alpha^2[C_2H_5O_2]^2 dx - \frac{k_{11}}{\alpha}\int_0^t \alpha[C_2H_5O_2]I(x)dx \equiv A \quad (19)$$

$$\alpha\int_0^t R_{production}(x)dx = I(t) + \frac{2k_7}{\alpha}\int_0^t I(x)^2 dx + \frac{k_{11}}{\alpha}\int_0^t \alpha[C_2H_5O_2]_x I(x)dx \equiv B \quad (20)$$

We initially assume $A_{(0)} = 0$, and then calculate the nth approximations to the quantities A and B using the following equations:

$$B_{(n)} = I(t) + \frac{2k_7}{\alpha}\int_0^t I(x)^2 dx + \frac{k_{11}}{\alpha}\int_0^t A_{(n)}I(x)dx \quad (21)$$

$$A_{(n+1)} = (I_{ref}(0) - B_{(n)}) - \frac{2k_{15}}{\alpha}\int_0^t (I_{ref}(0) - B_{(n)})^2 dx - \frac{k_{11}}{\alpha}\int_0^t (I_{ref}(0) - B_{(n)})I(x)dx \quad (22)$$

Iteration of these equations converges to a solution for B which represents the production of HO_2 from reaction 1 which would give rise to the observed signal under the conditions of the model. The yields extracted from this procedure are necessarily larger than the raw yields taken directly from the data (corrected only for self-reaction). Yield estimates based on both methods are given in Table 1.

The temperature dependence of the HO_2 yields for a constant total density is shown in Figure 5. The biexponential HO_2 production allows separation of prompt HO_2 from the remainder of the HO_2 product. The total yield, which includes the slower rise in HO_2, rises slowly at low temperatures but abruptly increases from 10% to 100% between 548 and 648 K. The prompt yield smoothly increases with temperature over the entire temperature range; the rapid increase is entirely from the delayed production of HO_2. This increase occurs at significantly higher temperatures than observed by Kaiser; however, the competing removal mechanisms for $C_2H_5O_2$ in this system are radical−radical reactions. The radical densities in Kaiser's smog chamber experiments are much lower than the $\sim 3-4 \times 10^{13}$ cm^{-3} in the present system, so the thermal dissociation does not overcome the competing reactions until higher temperatures in the current work. The circles with crosses in Figure 5 are yield measurements made at radical densities approximately 5 times higher ($\sim 2-3 \times 10^{14}$ cm^{-3}) than for most of the other experiments; the yield at high temperatures is significantly reduced for higher radical concentrations.

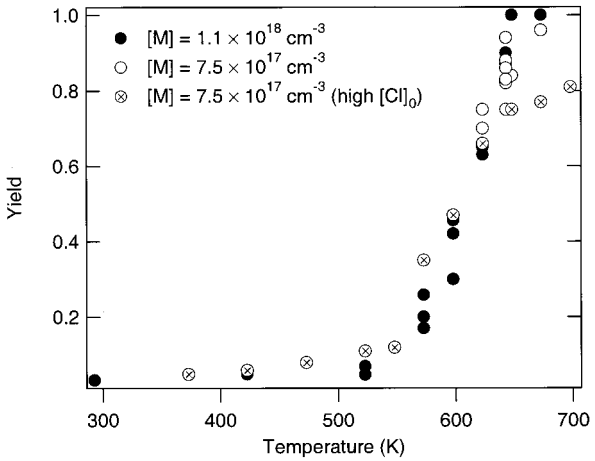

Figure 5. Measured total HO_2 yields as a function of temperature for total densities of 1.1×10^{18} cm^{-3} (solid circles) and 7.5×10^{17} cm^{-3} (open circles). The circles with the crosses represent experiments with higher initial Cl atom concentrations ($2-3 \times 10^{14}$ cm^{-3}). The reduction in yield at high temperatures for higher radical densities occurs because of increased removal of $C_2H_5O_2$ by radical−radical reactions before dissociation can occur.

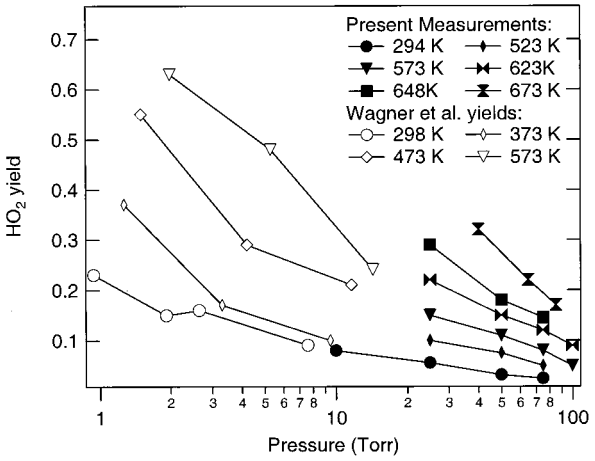

Figure 6. Pressure dependence of prompt HO_2 yields for several temperatures. The yield measurements of Wagner et al. (ref 11) are shown as the open symbols. The inverse pressure dependence of the prompt yields persists even at higher temperatures where the pressure dependence of the total yields, which include redissociation of $C_2H_5O_2$, are negligible.

The change in prompt HO_2 yield with total pressure is shown in Figure 6. As observed in previous experiments, the yield of HO_2 is inversely dependent on pressure in the low temperature regime, because stabilization of the ethylperoxy radical becomes increasingly dominant as the pressure is raised. At higher temperatures, stabilization becomes more difficult and thermal dissociation of the ethylperoxy radical begins to occur, and the dependence of the yield on pressure lessens. At the highest temperatures of the present studies the total HO_2 yield displays little or even a slight positive pressure dependence, due entirely to the pressure dependence of the delayed HO_2 production. However, the prompt yield retains its inverse pressure dependence even at the highest temperatures observed. The present results are in good agreement with extrapolation of published results at lower pressures, as can be seen in Figure 6.

Upper Limits on OH Yields. Detection of OH products from reaction 1 was attempted using infrared absorption on the $P(2.5)1^-$ line. A clear absorption signal could be detected from the reference system of $CH_2OH + O_2 + NO$ (reactions 4−6 above), which is used as a calibration for possible OH

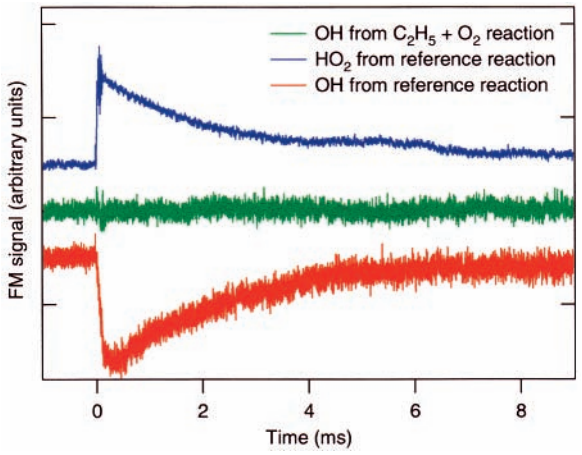

Figure 7. Simultaneous OH and HO_2 detection in the $Cl_2/CH_3OH/O_2/NO$ system and attempted detection of OH from $C_2H_5 + O_2$. No OH is observed under the conditions of the present study.

TABLE 2: Upper Limits for OH Yields from $C_2H_5 + O_2$

temp	prompt OH yield	delayed OH yield
523	≤0.02	≤0.1
573	≤0.03	≤0.1
700	≤0.06	≤0.15

production in reaction 1. Figure 7 illustrates the simultaneous detection of HO_2 and OH in the reference system. The time behavior of the HO_2 and OH signals can be modeled by a mechanism which contains reactions 2, 4−6, and additional reactions of OH with methanol and HO_2:

$$OH + CH_3OH \rightarrow H_2O + CH_2OH \text{ (or } CH_3O) \quad (23)$$

$$OH + HO_2 \rightarrow H_2O + O_2 \quad (24)$$

$$CH_3O + O_2 \rightarrow CH_2O + HO_2 \quad (25)$$

Figure 7 also shows an attempted measurement of OH production from reaction 1 at 623 K. Measurements at temperatures from 573 to 700 K and pressures of 25 and 50 Torr failed to produce observable OH within the noise limits of the experiment.

Assuming reactions 4−6 convert 100% of the initial Cl atoms to OH, the signal which would be observed for various OH yields in reaction 1 can be predicted. The mechanism is identical to that for the reference system, except that reaction 23 is replaced by reaction 26,

$$OH + C_2H_6 \rightarrow H_2O + C_2H_5 \quad (26)$$

and the NO concentration is zero. Upper limits to the OH yield are determined by considering the signal-to-noise ratio of the reference OH signal and the relative sensitivity to OH in the reference system and in the $Cl_2/C_2H_6/O_2$ system. The main determinant of the relative sensitivity is the production rate of OH relative to the removal by OH + ethane or OH + methanol reactions. A slower production of OH, as may occur after isomerization of thermalized ethylperoxy radicals, would produce smaller peak OH concentrations than immediate production from a direct reaction. Two separate upper limits for OH production are therefore listed in Table 2, one for prompt OH production, and a higher limit for delayed production on a time scale matching the slow rise in HO_2 signals. Walker and coworkers have measured stable products from the addition of ethane to reacting H_2/O_2 and 2,2,3,3-tetramethylbutane/O_2 mixtures and have deduced branching fractions for production of oxirane relative to ethylene.[12] The initial $[C_2H_4]/[C_2H_4O]$ ratios in those experiments, which range from 127 at 673 K to 87 at 813 K, are consistent with the upper limits to OH production observed at the lower temperatures of the present experiments.

TABLE 3: Time Constants for Delayed HO_2 Production as a Function of O_2 Concentration

temp (K)	$[O_2]$	τ
643	2.7×10^{15} cm^{-3}	84 s^{-1}
	5.3×10^{15} cm^{-3}	96 s^{-1}
	1.1×10^{16} cm^{-3}	107 s^{-1}
	1.1×10^{16} cm^{-3}	94 s^{-1}
	1.1×10^{16} cm^{-3}	118 s^{-1}
	2.1×10^{16} cm^{-3}	138 s^{-1}
	3.2×10^{16} cm^{-3}	91 s^{-1}
	4.3×10^{16} cm^{-3}	100 s^{-1}
	5.3×10^{16} cm^{-3}	93 s^{-1}
	6.4×10^{16} cm^{-3}	93 s^{-1}
658	5.1×10^{15} cm^{-3}	129 s^{-1}
	6.9×10^{15} cm^{-3}	114 s^{-1}
	1.1×10^{16} cm^{-3}	86 s^{-1}
	1.9×10^{16} cm^{-3}	140 s^{-1}
	6.7×10^{16} cm^{-3}	204 s^{-1}
	1.3×10^{17} cm^{-3}	140 s^{-1}
	1.8×10^{17} cm^{-3}	157 s^{-1}

Time Behavior of HO_2 Production. The time-resolved FM signal shown in Figure 4, after the correction for HO_2 self-reaction, is related to the production of HO_2 in reaction 1:

$$I_{\text{corrected}}(t) = \alpha \int_0^t R_{\text{production}}(x)\mathrm{d}x - \alpha \int_0^t R_{\text{removal}}(x)[HO_2]_x \mathrm{d}x \quad (27)$$

The effective time-resolved production and removal rates are composites of elementary rate processes. Under the conditions of our experiments R_{removal} is dominated by the reaction of HO_2 with $C_2H_5O_2$, as discussed above. The approximate correction for this reaction, made using the assumption that the steady-state of reaction 1a lies far to the right, is accomplished using the recursive solution of eqs 21 and 22, to extract an effective HO_2 profile which reflects only the production from reaction 1:

$$I_{\text{eff}}(t) \approx \alpha \int_0^t R_{\text{production}}(x)\mathrm{d}x \quad (28)$$

The present experiments require relatively large concentrations of O_2, because the signal size is determined by the initial Cl concentration (and hence the Cl_2 concentration), and $[O_2]$ is maintained at 30−100 $[Cl_2]$. As a result, the initial rise of HO_2 from the reaction of ethyl with O_2 is rapid and unresolved. However, the slower time constant, τ, in the production of HO_2 can be measured, and time constants are listed in Tables 1 and 3. Figure 8 shows the slow time constant, extracted from the effective signals after correction for self-reaction and the $HO_2 + C_2H_5O_2$ reaction (reaction 11), as a function of temperature. The time constant displays a rapid increase from approximately 30 s^{-1} at 573 K to several hundred per second at 698 K. The lowest temperature time constants are slightly affected by the correction for reaction 11, but at higher temperatures this correction is less important and the time constants are independent of the details of the HO_2 removal mechanism. At 623 K, a change of 50% in the assumed rate coefficient for reaction 11 changes the extracted time constant by approximately 5%.

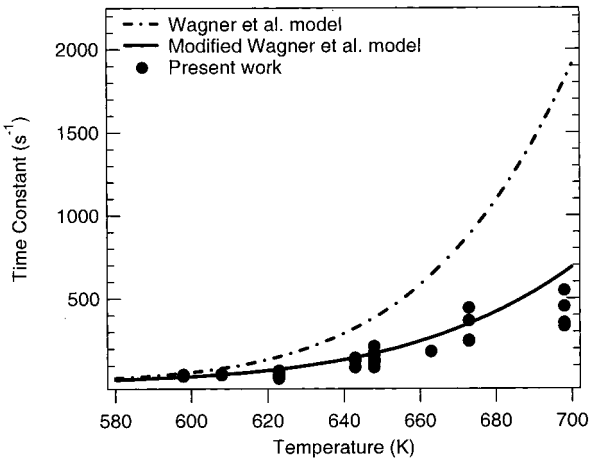

Figure 8. Time constant τ for delayed production of HO_2 as a function of temperature. The dot−dashed line shows the predictions of the parameterization of the $C_2H_5 + O_2$ reaction published by Wagner et al. (ref 11). The solid line is the predictions of the same model after an ad hoc correction to account for recent equilibrium constant measurements. See text for details.

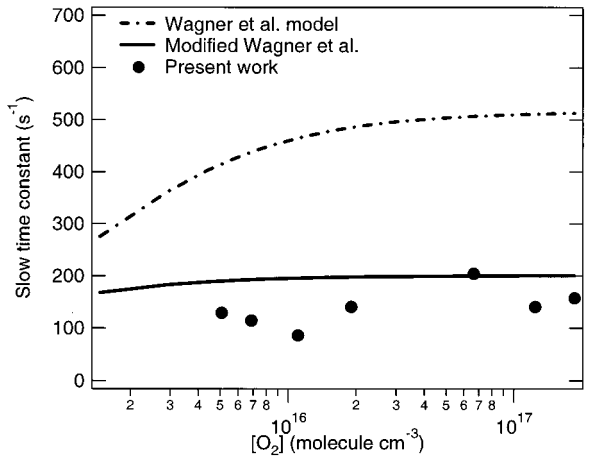

Figure 9. Time constant τ as a function of O_2 concentration at 658 K. The dot−dashed line shows the predictions of the parameterization of the $C_2H_5 + O_2$ reaction published by Wagner et al. (ref 11). The solid line is the predictions of the same model after an ad hoc correction to account for recent equilibrium constant measurements. See text for details.

Time constants have been measured as a function of oxygen concentration (Table 3) and total pressure. Figure 9 shows the time constants measured for various partial pressures of O_2 at 658 K and total density of 8.5×10^{17} cm^{-3}. The time constant shows no dependence on the oxygen concentration at the relatively high $[O_2]$ used in these experiments. The effect of total pressure on the slow time constant is also observed to be small in the 25−85 Torr pressure range of the present experiments, as shown in Figure 10 for 643 K.

Discussion

The description of reaction 1 must reflect the complex dependences of the time behavior and the HO_2 yields on pressure and temperature. The main features of the reaction can be made plain by first applying a simplified analytical model to the reaction, where the measured quantities can be related to explicit convolutions of elementary kinetic steps. This is the strategy employed by Wagner et al. in their parameterization of the $C_2H_5 + O_2$ reaction.[11] Reaction 1 is known to proceed through the intermediate $C_2H_5O_2$, and a simplified formal kinetic scheme

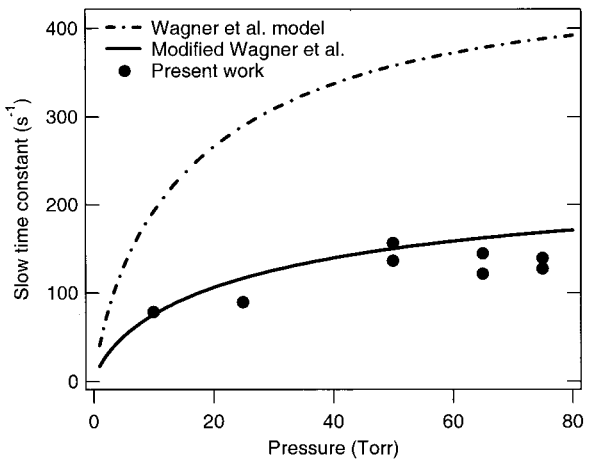

Figure 10. Pressure dependence of the time constant τ for delayed production of HO_2. The dot−dashed line shows the predictions of the parameterization of the $C_2H_5 + O_2$ reaction published by Wagner et al. (ref 11). The solid line is the predictions of the same model after an ad hoc correction to account for recent equilibrium constant measurements. See text for details.

for the reaction can be constructed using only the species in reactions 1a and 1b:

$$C_2H_5 + O_2 \xrightarrow{k_a} C_2H_4 + HO_2$$

$$C_2H_5 + O_2 \underset{}{\overset{k_{1a}[M]}{\longleftrightarrow}} C_2H_5O_2 \xrightarrow{k_e[M]} C_2H_4 + HO_2 \qquad (29)$$

$$\downarrow$$

$$\text{removal}$$

where k_e represents elimination from $C_2H_5O_2$ and k_a represents a direct production of HO_2 and ethylene from the reactants. The direct reaction does not necessarily represent an abstraction reaction, but any immediate production of HO_2 and C_2H_4, including rapid dissociation of an incipient $C_2H_5O_2$ complex before collisional stabilization. A similar scheme has been used by Wagner et al.[11]

In general, the kinetics of Scheme 29 give a biexponential production of HO_2 products, where the time constants and amplitudes depend on all the rate coefficients of the system. The parameterization of reaction 1 using phenomenological rate coefficients for the mechanism 29 allows a qualitative understanding of the reaction mechanism. The measured HO_2 production can be described by the rapid establishment of a steady state in reaction 1a, followed by a slow production of HO_2 with a time constant reflecting the removal rate of $C_2H_5O_2$. Using the coupled mechanism for reaction 1, as depicted in Figure 11, the significance of the experimentally accessible quantities can be described. The fast time constant, reflecting the establishment of the steady state between addition and redissociation, is governed by the transition state for addition, TS1. The prompt yield, which is the fraction of HO_2 at the establishment of the steady-state, reflects the competition between collisional stabilization and elimination via the second transition state TS2. The slow time constant depends on the escape of radicals from the $C_2H_5 + O_2 \leftrightarrow C_2H_5O_2$ quasi-equilibrium through TS2, both by the "direct" reaction with rate coefficient k_a and by thermal elimination. Recently, Miller et al. performed detailed master equation calculations that give a physically rigorous description of the competition between stabilization and elimination.[17] Their results demonstrate the dominance of the second transition state in determining the rate coefficient above 700 K, where the stabilization channel ceases to play a role.

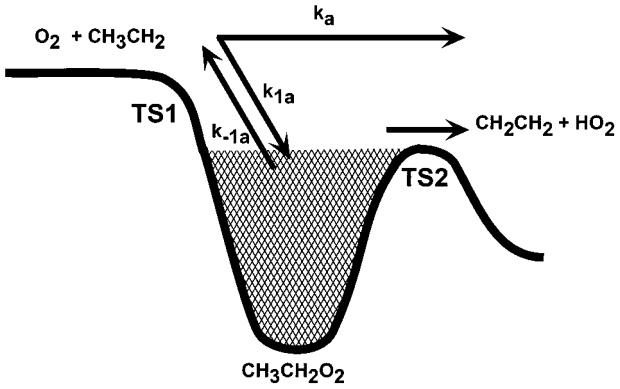

Figure 11. Simplified schematic representation of the reaction mechanism for $C_2H_5 + O_2$. Several other potential wells and transition states exist in the $C_2H_5O_2$ system, but do not affect the present experiments.

The parameterization of reaction 1 provided by Wagner et al.[11] is readily applied to modeling the present results. Kaiser has also used this parameterization to describe his measurements of ethylene yields as a function of temperature.[21] However, the equilibrium constants which formed part of the basis of this model have recently been substantially revised.[19] The time constant for the delayed production of HO_2 is sensitive to the dissociation pathways of the ethylperoxy radical. Figure 8 shows the measured effective time constants for the slow production of HO_2 as a function of temperature in the present experiments. The predictions of the original Wagner et al. parameterization are shown as the dot−dashed line. (Note that the activation energies of k_0 and k_∞ for $C_2H_5O_2 \rightarrow C_2H_4 + HO_2$ should be positive, not negative as printed in Table 6 of ref 11)[39] This model predicts a far more rapid dissociation of the $C_2H_5O_2$ radical at these temperatures than is experimentally observed. However, this overestimation is not completely unexpected, given that the equilibrium constants predicted by the Wagner et al. model have since been shown to be in error by up to a factor of 5. An ad hoc modification to the Wagner et al. parameterization can be constructed by simply correcting the rate coefficient for the reverse reaction to match the reevaluated equilibrium constants. As the simplest approximation, we have simply fit the correction factors $K_{eq,new}/K_{eq,old}$ from the reanalyzed equilibrium data[19] to an Arrhenius form and used this expression to modify the rate coefficient k_{-1a} (k_{-4a} in ref 11). This fit yields $k_{-1a,new}/k_{-1a,old} = 1.16 \times 10^{-3}\ e^{3480/T}$; the experimental equilibrium constants and the predictions of the modified parameterization are shown in Figure 12. Application of this ad hoc correction to the calculation of the slow time constant yields predictions which are in much better agreement with the experimentally observed quantities, as shown by the solid line in Figure 8. The negligible dependence of the time constant on O_2 concentration is duplicated by the analytic model, as shown in Figure 9. The modified parameterization also predicts a very shallow pressure dependence, in agreement with the observations shown in Figure 10.

Master equation calculations have been carried out recently by Miller, Klippenstein, and Robertson, on the basis of quantum chemical calculations of the transition state for HO_2 elimination from the ethylperoxy radical.[17] These calculations employ a transition state TS2 which is −4.3 kcal mol^{-1} from the energy of the $C_2H_5 + O_2$ reactants, an energy which was adjusted to fit the high-temperature rate coefficient measurements of Gutman and co-workers. The second transition state completely determines the high-temperature rate coefficient as stabilization becomes negligible. Calculations using this transition state predict time constants in excellent agreement with the present measurements.[40] Both the high-temperature rate coefficient and the slow time constant are sensitive to the energy of the elimination transition state TS2. The agreement between the present experiments and the master equation calculations therefore demonstrates consistence between the time constant measurements and the literature values for the high-temperature rate coefficient. By extension, the time constant measurements also provide further evidence for the direct elimination mechanism used in the master equation calculations.

Analysis of the HO_2 yields is somewhat more problematic. The parameterization does not include any irreversible removal of ethyl radicals except by reaction to form HO_2 and ethylene. The yield as $t \rightarrow \infty$ is therefore always unity. Comparison to experimental results requires estimation of the competing reactions of the stabilized $C_2H_5O_2$ radical, designated "removal" in eq 29. This can be accomplished, as in the original Wagner et al. work, by introducing a "cutoff" time, corresponding to some experimental limiting time scale, at which the yield will be evaluated. Unless this time is unambiguously defined by the experiments, this approach essentially introduces an arbitrary fitting parameter, which determines the temperature at which the rapid rise in yield is predicted. In the evaluation of his smog chamber measurements of C_2H_4 yields in reaction 1, Kaiser employed a more detailed modeling of the chemistry, using a 12-reaction kinetic mechanism. Application of a similar mechanism enables a relatively direct comparison between the experimental measurements and the parameterization used to model the $C_2H_5 + O_2$ reaction. The model presently employed, given in Table 4, assumes no production of C_2H_4OOH radical as a precursor to $C_2H_4 + HO_2$, which is consistent with recent calculations of a direct pathway for HO_2 elimination from $C_2H_5O_2$.[14−17]

Because the removal of $C_2H_5O_2$ is dominated by radical−radical reactions, the predictions of the chemical kinetic model in Table 4 depend sensitively on the initial radical density, $[C_2H_5]_0 = [Cl]_0$. This dependence is manifested experimentally in the dependence of the yield on initial Cl concentration, as shown in Figure 5. The initial radical density is measured in the present experiments via the second-order decay of the reference signal. Using literature values for k_7, the initial HO_2 density can be calculated for the reference system, which is equal to the initial ethyl radical density in the ethyl + O_2 measurement. The time-resolved HO_2 signal can then be calculated, using literature values for the rate coefficients and the experimentally determined radical density. Figure 13 shows a comparison between calculated signals (with the HO_2 self-reaction removed) and the experimental signals corrected only for HO_2 self-reaction. The calculated time trace is completely specified by the model and the initial radical density from the reference reaction measurement, leaving no adjustable parameters. Once again the overestimation of $C_2H_5O_2$ dissociation in the original model of Wagner et al. is evident in the comparison to the experimental data. The ad hoc correction for the reevaluated equilibrium constants yields predictions that are in much better agreement with the experiments.

The correspondence between the experimental $[HO_2]$ vs time profiles and the predictions of the ad hoc model which is shown in Figure 13 is typical of the agreement for measurements in the transition region between 600 and 650 K, where the total HO_2 yields are intermediate between the low prompt yields observed at lower temperatures and the ∼100% yields observed at higher temperatures. Slight systematic differences persist as evident in the figure; the prompt yields are slightly underpre-

TABLE 4: Kinetic Model for $Cl_2/C_2H_6/O_2$ System

reaction	rate coefficient	ref
$Cl + C_2H_6 \rightarrow C_2H_5 + HCl$	$8.5 \times 10^{-11}\, e^{-113/T}$ cm^3 molecule^{-1} s^{-1}	24
$C_2H_5 + Cl_2 \rightarrow C_2H_5Cl + Cl$	$1.26 \times 10^{-11}\, e^{152/T}$ cm^3 molecule^{-1} s^{-1}	41
$HO_2 + HO_2 \rightarrow H_2O_2 + O_2$	1.2×10^{-33} [M] $e^{1150/T} + 3.8 \times 10^{-13}\, e^{580/T}$ cm^3 molecule^{-1} s^{-1}	42
$C_2H_5 + O_2 \rightarrow C_2H_5O_2$[a]	$\phi = 1 - \{(1 + e^{2.3c_3 + c_4c_3^2})^{0.621}\}^{-1}$; $c_3 = \log([M]) - 15.53 - 3.11 \times 10^{-4}T - 1.54 \times 10^{-6}T^2$ $c_4 = 0.367 - 7.09 \times 10^{-4}T + 3.23 \times 10^{-7}T^2$ $k_\infty = 3.67 \times 10^{-14}T^{0.772}e^{287/T}$; $k_0 = 1.96 \times 10^{-5}T^{-8.24}e^{-2150/T}$; $F_{cent} = 0.580e^{-T/1250} + 0.420e^{-T/183}$	11
$C_2H_5 + O_2 \rightarrow C_2H_4 + HO_2$[a]	$\phi = \{(1 + e^{2.3c_3 + c_4c_3^2})^{0.621}\}^{-1}$; $c_3 = \log([M]) - 15.53 - 3.11 \times 10^{-4}T - 1.54 \times 10^{-6}T^2$ $c_4 = 0.367 - 7.09 \times 10^{-4}T + 3.23 \times 10^{-7}T^2$ $k_\infty = 3.67 \times 10^{-14}T^{0.772}e^{287/T}$; $k_0 = 1.96 \times 10^{-5}T^{-8.24}e^{-2150/T}$; $F_{cent} = 0.580e^{-T/1250} + 0.420e^{-T/183}$	11
$C_2H_5O_2 \rightarrow C_2H_5 + O_2$[a]	$\phi = 1.16 \times 10^{-3}e^{3480/T}$ (ad hoc correction); $\phi = 1$(original model); $k_\infty = 6.17 \times 10^{17}T^{-0.835}e^{-17160/T}$; $k_0 = 3.29 \times 10^{26}T^{-9.85}e^{-19600/T}$; $F_{cent} = 0.580e^{-T/1250} + 0.420e^{-T/183}$	11
$C_2H_5O_2 \rightarrow C_2H_4 + HO_2$[a]	$\phi = 1$; $k_\infty = 6.92 \times 10^{14}T^{-0.634}e^{-15800/T}$; $k_0 = 2.04 \times 10^{35}T^{-12.86}e^{-20100/T}$; $F_{cent} = 2.72e^{-T/220} + e^{-7270/T}$	11,39
$C_2H_5O + O_2 \rightarrow HO_2 + CH_3CHO$	$6.0 \times 10^{-14}\, e^{-550/T}$ cm^3 molecule^{-1} s^{-1}	43
$C_2H_5O_2 + C_2H_5O_2 \rightarrow 2C_2H_5O + O_2$	$(1.33\, e^{-207/T})\, 8.5 \times 10^{-14}\, e^{-125/T}$ cm^3 molecule^{-1} s^{-1}	44
$C_2H_5O_2 + C_2H_5O_2 \rightarrow CH_3CHO + C_2H_5OH + O_2$	$(1-1.33\, e^{-207/T})\, 8.5 \times 10^{-14}\, e^{-125/T}$ cm^3 molecule^{-1} s^{-1}	44
$C_2H_5O_2 + HO_2 \rightarrow C_2H_5O_2H + O_2$	$2.7 \times 10^{-13}\, e^{1000/T}$ cm^3 molecule^{-1} s^{-1}	43
$C_2H_5O_2H \rightarrow C_2H_5O + OH$	$4.0 \times 10^{15}\, e^{-21600/T}$ s^{-1}	45

[a] Rate coefficient is parameterized using the listed parameters in the expressions

$$k = \phi \frac{k_\infty k_0[M]}{k_\infty + k_0[M]}(F_{cent})^c;\ c^{-1} = 1 + \left\{ \frac{\log\left[\frac{k_0[M]}{k_\infty}\right] - 0.4 - 0.67\log[F_{cent}]}{0.75 - 1.27\log[F_{cent}] - 0.14\left(\log\left[\frac{k_0[M]}{k_\infty}\right] - 0.4 - 0.67\log[F_{cent}]\right)} \right\}^2$$

with the values for the parameters as given.

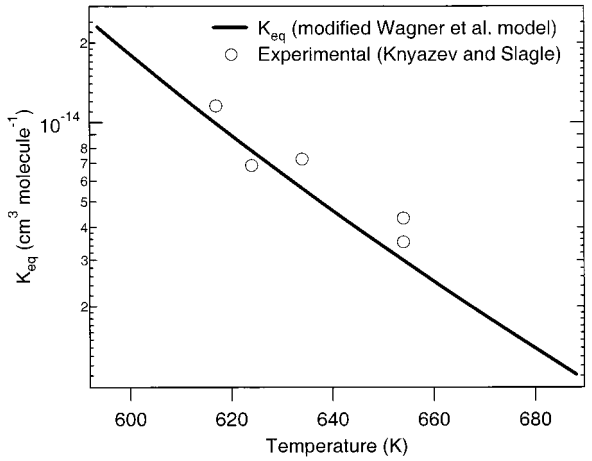

Figure 12. Comparison of equilibrium constants for reaction 1a reported by Knyazev and Slagle (ref 19) with those predicted by the Wagner et al. parameterization after adjustment of the rate constant k_{1a}. See text for details.

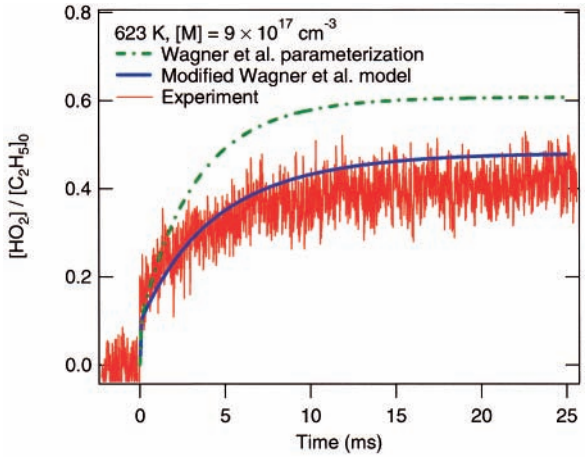

Figure 13. Comparison of time-resolved HO_2 signal with predicted signals based on the analytic model for the $Cl_2/C_2H_6/O_2$ system (Table 4). The initial radical density (equal to the initial Cl atom concentration) is fixed by the second-order decay of the associated reference reaction signal, leaving no adjustable parameters for the model signal. The dot–dashed line shows the predictions of the parameterization of the $C_2H_5 + O_2$ reaction published by Wagner et al. (ref 11). The solid line is the predictions of the same model after an ad hoc correction to account for recent equilibrium constant measurements. See text for details.

dicted and the time constant is still on average somewhat overpredicted, even by the corrected model. At higher temperatures the model fails to predict yields reaching 100%, probably because the kinetic significance of the ethylperoxy adduct is overestimated in the model; in particular the extrapolation of the $C_2H_5O_2 + HO_2$ reaction rate coefficient may be unreliable. However, the general agreement obtained from a simple modification to the Wagner et al. parameterization is good.

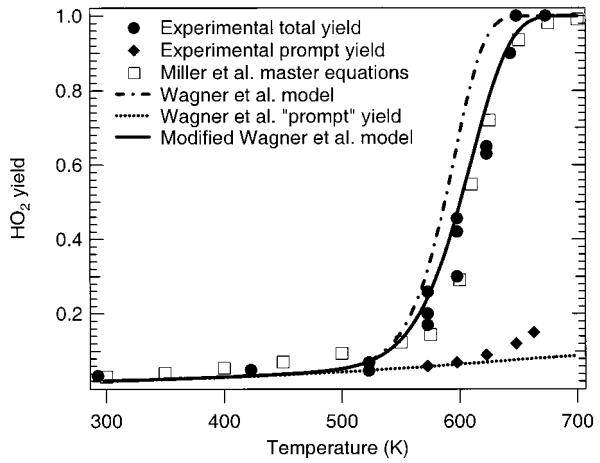

Figure 14. Predictions of HO_2 yields at a total density of 1.1×10^{18} cm^{-3} as a function of temperature from the parameterization of the $C_2H_5 + O_2$ reaction. The experimental yields are shown as the solid circles. The master equation calculations of Miller and co-workers (ref 17) are shown as the open squares. The dot−dashed line shows the predictions of the parameterization of the $C_2H_5 + O_2$ reaction published by Wagner et al. (ref 11). The solid line is the predictions of the same model after an ad hoc correction to account for recent equilibrium constant measurements. See text for details.

Finally in Figure 14 the experimental HO_2 yields are compared to predictions based on the analytic parameterization. The cutoff time has been chosen to be 17 ms to best match the predictions of the corrected model with the measured HO_2 yields. As can be seen in Figure 13, the delayed production of HO_2 is largely complete in 15−20 ms at the temperatures that characterize the rapid increase in HO_2 yield. For comparison, the predictions of the original Wagner et al. model are also shown. The agreement of the measured yields with the model predictions is quite satisfactory, although, as mentioned above, there is an element of arbitrariness in the comparison arising from the choice of cutoff times. The comparisons of model predictions to experimental time constants and to the actual data traces are a more reliable indicator of the success of the corrected parameterization.

Also shown in Figure 14 are comparisons with calculated yields reported by Miller et al. and based on master equation simulations.[17] The results of their calculations are once again in outstandingly good agreement with the experimental measurements. The master equation analysis rigorously describes the competition between stabilization and elimination without recourse to a phenomenological effective kinetic scheme. Miller et al. have provided expressions for the high and low pressure limiting rate coefficients for reaction 1 as a function of temperature. The results of master equation calculations could also be used, possibly in conjunction with additional experimental measurements, to construct a new parameterization for the falloff behavior of reaction 1 in the transition temperature region. Such an undertaking is, however, far beyond the scope of the present work. The ad hoc correction to the falloff parameterization of Wagner et al. appears to acceptably model the present experimental data in the temperature region up to approximately 700 K. At higher temperatures the reaction should be described well by the pressure-independent bimolecular expression given by Miller et al.

The present data appear in excellent agreement with the predictions of a coupled kinetics model where the formation of an ethylperoxy radical is the antecedent to ethylene + HO_2 formation. The separation of time scales for HO_2 production in the present results permits separation of prompt HO_2 formation from formation via thermal dissociation of the $C_2H_5O_2$. This kinetic signature demonstrates unambiguously that the rapid rise in HO_2 yields with temperature arises from the redissociation of the ethylperoxy radical. The prompt yields rise slightly with temperature from 298 to 700 K and show an inverse pressure dependence over the entire temperature range. The pressure dependence of the prompt yield derives from the competition between elimination and collisional stabilization in the initially formed excited adduct. Neither the rapid rise in total HO_2 yield nor the rise in prompt yield at elevated temperatures appears to be a result of the emergence of the direct abstraction pathway. The master equation calculations of the high-temperature rate coefficient, the HO_2 yields, and the slow time constant for HO_2 formation by Miller and co-workers display a high degree of sensitivity to the energy of the transition state to elimination.[17,40] Their transition state energy of -4.3 kcal mol^{-1}, chosen to match the high temperature rate measurements, produces nearly exact agreement with the present yield and time constant measurements. The level and scope of the conformity of theory and experiment provide strong evidence of the accuracy of this description. While the understanding of the $C_2H_5 + O_2$ reaction may appear complete in this temperature region, further experimental and theoretical studies aimed at the reverse reaction, $C_2H_4 + HO_2$, and at temperatures above 1000 K may provide information concerning other areas of the potential energy surface and could help resolve remaining questions about this complex chemical reaction.

Conclusions

The reaction of ethyl radicals with O_2 has been investigated as a function of temperature between 293 and 698 K using laser photolysis/CW frequency modulation spectroscopy. The yield of HO_2 in the reaction shows a rapid increase between 600 and 650 K, which is attributable to the onset of thermal dissociation of the ethylperoxy radical. The experimental results can be successfully modeled using the parameterization of Wagner et al. if a modification is made to correct the predicted equilibrium constants. Recent master equation calculations are in excellent agreement with the present experimental results, consistent with the $C_2H_5 + O_2 \rightarrow C_2H_4 + HO_2$ reaction proceeding via a concerted elimination with a transition state ~4.3 kcal mol^{-1} below the reactants.

Acknowledgment. The experiments described here were made possible by the able technical support of Leonard E. Jusinski. The authors thank Dr. James A. Miller and Prof. Stephen J. Klippenstein for illuminating discussions regarding master equation modeling of the ethyl + O_2 reaction and for sharing results of their calculations prior to publication. This work is supported by the Division of Chemical Sciences, the Office of Basic Energy Sciences, the U.S. Department of Energy.

References and Notes

(1) Robertson, S. H.; Seakins, P. W.; Pilling, M. J. In *Low-Temperature Combustion and Autoignition*; Pilling, M. J., Ed.; Elsevier: Amsterdam, 1997; Vol. 35, p 125.

(2) Walker, R. W. In *Research in Chemical Kinetics*; Compton, R., Hancock, G., Eds.; Elsevier: Amsterdam, 1995; Vol. 3, p 1.

(3) Walker, R. W.; Morley, C. In *Low-Temperature Combustion and Autoignition*; Pilling, M. J., Ed.; Elsevier: Amsterdam, 1997; Vol. 35, p 1.

(4) Plumb, I. C.; Ryan, K. R. *Int. J. Chem. Kinet.* **1981**, *13*, 1011.

(5) Kaiser, E. W.; Lorkovic, I. M.; Wallington, T. J. *J. Phys. Chem.* **1990**, *94*, 3352.

(6) Kaiser, E. W.; Wallington, T. J.; Andino, J. M. *Chem. Phys. Lett.* **1990**, *168*, 309.

(7) Kaiser, E. W.; Rimai, L.; Wallington, T. J. *J. Phys. Chem.* **1989**, *93*, 4094.
(8) Slagle, I. R.; Feng, Q.; Gutman, D. *J. Phys. Chem.* **1984**, *88*, 3648.
(9) McAdam, K. G.; Walker, R. A. *J. Chem. Soc., Faraday Trans. 2* **1987**, *83*, 1509.
(10) Bozzelli, J. W.; Dean, A. M. *J. Phys. Chem.* **1990**, *94*, 3313.
(11) Wagner, A. F.; Slagle, I. R.; Sarzynski, D.; Gutman, D. *J. Phys. Chem.* **1990**, *94*, 1853.
(12) Baldwin, R. R.; Pickering, I. A.; Walker, R. W. *J. Chem. Soc., Faraday Trans. 1* **1980**, *76*, 2374.
(13) Baldwin, R. R.; Stout, D. R.; Walker, R. W. *J. Chem. Soc., Faraday Trans.* **1991**, *87*, 2147.
(14) Quelch, G. E.; Gallo, M. M.; Schaefer, H. F., III *J. Am. Chem. Soc.* **1992**, *114*, 8239.
(15) Quelch, G. E.; Gallo, M. M.; Shen, M.; Xie, Y.; Schaefer, H. F., III; Moncrief, D. *J. Am. Chem. Soc.* **1994**, *116*, 4953.
(16) Ignatyev, I. S.; Xie, Y.; Allen, W. D.; Schaefer, H. F., III *J. Chem. Phys.* **1997**, *107*, 141. Rienstra-Kiracofe, J. C.; Allen, W. D.; Schaefer, H. F., III *J. Phys. Chem. A* **2000**, *104*, 9823.
(17) Miller, J. A.; Klippenstein, S. J.; Robertson, S. H. *Proc. Symp. (International) Combust.* **2000**, *28*, in press.
(18) Chen, C.-J.; Bozzelli, J. W. *J. Phys. Chem. A* **2000**, *104*, 4997.
(19) Knyazev, V. D.; Slagle, I. R. *J. Phys. Chem. A* **1998**, *102*, 1770.
(20) Slagle, I. R.; Ratajczak, E.; Gutman, D. *J. Phys. Chem.* **1986**, *90*, 402.
(21) Kaiser, E. W. *J. Phys. Chem.* **1995**, *99*, 707.
(22) Pilgrim, J. S.; Taatjes, C. A. *J. Phys. Chem. A* **1997**, *101*, 5776.
(23) Pilgrim, J. S.; Taatjes, C. A. *J. Phys. Chem. A* **1997**, *101*, 4172.
(24) Pilgrim, J. S.; McIlroy, A.; Taatjes, C. A. *J. Phys. Chem. A* **1997**, *101*, 1873.
(25) Pilgrim, J. S.; Taatjes, C. A. *J. Phys. Chem. A* **1997**, *101*, 8741.
(26) Farrell, J. T., Taatjes, C. A. *J. Phys. Chem. A.* **1998**, *102*, 4846.
(27) Becker, K. H.; Fink, E. H.; Langen, P.; Schurath, U. *J. Chem. Phys.* **1974**, *60*, 4623.
(28) Hunziker, H. E.; Wendt, H. R. *J. Chem. Phys* **1974**, *60*, 4622.
(29) Johnson, T. J.; Wienhold, F. G.; Burrows, J. P.; Harris, G. W.; Burkhard, H. *J. Phys. Chem.* **1991**, *95*, 6499.
(30) Amano, T. *J. Mol. Spectrosc.* **1984**, *103*, 436.
(31) Janik, G. R.; Carlisle, C. B.; Gallagher, T. F. *J. Opt. Soc. Am. B* **1986**, *3*, 1070.
(32) Herriott, D.; Kogelnik, H.; Kompfner, R. *Appl. Opt.* **1964**, *3*, 523.
(33) Pilgrim, J. S.; Jennings, R. T.; Taatjes, C. A. *Rev. Sci. Instrum.* **1997**, *68*, 1875.
(34) DeMore, W. B.; Sander, S. P.; Golden, D. M.; Hampson, R. F.; Kurylo, M. J.; Howard, C. J.; Ravishankara, A. R.; Kolb, C. E.; Molina, M. J. *Chemical Kinetics and Photochemical Data for Use in Stratospheric Modeling*; Jet Propulsion Laboratory: Pasadena, CA, 1997.
(35) Howard, C. J. *J. Am. Chem. Soc.* **1980**, *102*, 6937.
(36) Yamasaki, K.; Watanabe, A.; Kakuda, T.; Ichikawa, N.; Tokue, I. *J. Phys. Chem. A* **1999**, *103*, 451.
(37) Yamasaki, K.; Watanabe, A. *Bull. Chem. Soc. Jpn.* **1997**, *70*, 89.
(38) Yamasaki, K.; Watanabe, A.; Kakuda, T.; Tokue, I. *Int. J. Chem. Kinet.* **1998**, *30*, 47.
(39) Wagner, A. F.; Slagle, I. R.; Sarzynski, D.; Gutman, D. *J. Phys. Chem.* **1991**, *95*, 1014.
(40) Miller, J. A., private communication.
(41) Timonen, R. S.; Gutman, D. *J. Phys. Chem.* **1986**, *90*, 2987.
(42) Lightfoot, P. D.; Veyret, B.; Lesclaux, R. *J. Phys. Chem.* **1990**, *94*, 708.
(43) Atkinson, R.; Baulch, D. L.; Cox, R. A.; Hampson, R. F., Jr.; Kerr, J. A.; Rossi, M. J.; Troe, J. *J. Phys. Chem. Ref. Data* **1997**, *26*, 521.
(44) Wallington, T. J.; Dagaut, P.; Kurylo, M. J. *Chem. Rev.* **1992**, *92*, 667.
(45) Baulch, D. L.; Cobos, C. J.; Cox, R. A.; Frank, P.; Hayman, G.; Just, T.; Kerr, J. A.; Murrells, T.; Pilling, M. J.; Troe, J.; Walker, R. W.; Warnatz, J. *J. Phys. Chem. Ref. Data* **1994**, *23*, 847.